Dual-Polarization GNSS-R Interference Pattern Technique for Soil Moisture Mapping

Alberto Alonso Arroyo, *Student Member, IEEE,* Adriano Camps, *Fellow, IEEE,* Albert Aguasca, *Member, IEEE,* Giuseppe F. Forte, *Member, IEEE,* Alessandra Monerris, *Member, IEEE,* Cristoph Rüdiger, *Member, IEEE,* Jeffrey P. Walker, Hyuk Park, *Member, IEEE,* Daniel Pascual, *Student Member, IEEE,* and Raul Onrubia, *Student Member, IEEE*

***Abstract*—The interference pattern technique (IPT) consists of the coherent addition of the direct and reflected global navigation satellite systems (GNSS) signals in the receiving antenna. The detected power oscillates (fading), and the amplitude of these oscillations is very sensitive to the soil reflection coefficient at the specular reflection point. Therefore, variations of the reflection coefficient can be mapped, and thus dielectric constant variations, from which soil moisture can be retrieved. This work extends the use of the IPT technique from vertical polarization (V-Pol) to horizontal polarization (H-Pol). Moreover, the IPT equations are reformulated to facilitate the combination of dual-polarization retrievals. Simulations of the interference patterns at V- and H-Pol are presented for different soil moisture conditions. An upgrade of the SMIGOL GNSS-R instrument for dual-polarization observations is presented. This instrument was deployed in a flat, dry grassland in Yanco, Australia, in order to validate the proposed concepts. Finally, a comparison between the data retrieved from the SMIGOL instrument and the ground-truth soil moisture data is presented showing a good agreement between them and rainfall information.**

***Index Terms*—Brewster angle, global navigation satellite systems (GNSS), GNSS reflectometry (GNSS-R), interference pattern technique (IPT), soil moisture (SM).**

NOMENCLATURE

GPS	Global positioning system.
GNSS	Global navigation satellite systems.
GNSS-R	GNSS-reflectometry.
PARIS	PAssive Reflectometry and Interferometry System.
DDM	Delay-Doppler map.
EM	Electro-magnetic.
WAF	Woodward ambiguity function.
IPT	Interference pattern technique.
LHCP	Left hand circular polarization.
RHCP	Right hand circular polarization.
SM	Soil moisture.
SMIGOL	SM IPT GNSS Observations at L-Band.
V	Vertical.
H	Horitzontal.
SAR	Synthetic aperture radar.
ICF	Interferometric complex field.
RF	Radio frequency.
WP	Waveform peak.
VSWR	Voltage standing wave ratio.
P-SMIGOL	Polarimetric SMIGOL.
ESA	European Space Agency.

Manuscript received October 31, 2013; revised March 05, 2014; accepted April 23, 2014. This work was supported in part by the Spanish Ministry of Science and Innovation, "AROSA-Advanced Radio Ocultations and Scatterometry Applications using GNSS and other opportunity signals," code AYA2011-29183-C02-01/ESP, in part by a Monash University Faculty of Engineering Seed Grant 2013, in part by ACROSS (Advanced Remote Sensing Ground-Truth Demo and Test Facilities), in part by TERENO (Terrestrial Environmental Observatories) funded by the German Helmholtz-Association, in part by the CosmOz network and the funding provided by the Commonwealth Scientific and Industrial Research Organisation, and in part by the OzNet hydrological monitoring network.

A. A. Arroyo, A. Camps, A. Aguasca, G. F. Forte, H. Park, D. Pascual, and R. Onrubia are with the Department of Signal Theory and Communications, Universitat Politècnica de Catalunya-BarcelonaTech (UPC), Barcelona 08034, Spain (e-mail: alberto.alonso.arroyo@tsc.upc.edu; camps@tsc.upc.edu; aguasca@tsc.upc.edu; giuseppe.forte@tsc.upc.edu; park.hyuk@tsc.upc.edu; daniel.pascual@tsc.upc.edu; onrubia@tsc.upc.edu).

A. Monerris, C. Rüdiger, and J. P. Walker are with the Department of Civil Engineering, Monash University, Melbourne 3168, Australia (e-mail: sandra.monerris-belda@monash.edu; chris.rudiger@monash.edu; jeff.walker@monash.edu).

Color versions of one or more of the figures in this paper are available online at http://ieeexplore.ieee.org.

Digital Object Identifier 10.1109/JSTARS.2014.2320792

I. INTRODUCTION

SOIL MOISTURE is one of the key parameters in the global water cycle, and is highly related to the global climate [1]. SM monitoring at a global scale is only possible using remote sensing techniques. Optical, thermal infrared or microwave frequencies have been used in the past for its retrieval [2], with each of them having its individual advantages and limitations. Microwave remote sensing at L-band (1–2 GHz) is preferred because the atmosphere is nearly transparent to EM waves, the vegetation layer is semi-opaque up to $\sim 5\ \mathrm{kg/m^2}$ vegetation water content, and the sensitivity to changes in the dielectric constant of the observed object, and hence in SM, is very large. Active and passive sensors operating in this spectrum band have been successfully used in the past, including GNSS-R in recent years. SAR systems rely on backscattering measurements obtaining very high spatial resolution, but have relatively poor accuracy due to surface roughness effects. Microwave radiometers measure the thermal radiation of the surface [3]. In contrast to SAR, radiometers have higher accuracy, but suffer from poor spatial resolution [2] and potential radio-frequency interference issues. Microwave reflectometers rely on forward scattering measurements of opportunity signals in a bistatic configuration, such as those from GPS satellites. The ground resolution, which is known from bistatic SAR theory [4], [5], is higher than for radiometers, but lower than for SAR due to the shorter coherent integration time. The accuracy, as

for SARs, also suffers from surface roughness, as they are based on similar physical principles.

The concept of GNSS-R started in 1991, when a French military plane testing a GPS receiver got locked to the reflected GPS signals over the ocean, leading to an incorrect navigation solution [6]. In 1993, the PARIS concept was proposed by the ESA, which consisted of using GNSS-reflected signals for multipoint mesoscale altimetry. This is considered to be the beginning of the GNSS-R techniques [7]. Since then, several uses of the GNSS-reflected signals have been proposed for a wide range of applications [8]–[10].

The retrieval of SM using GNSS-R has been widely addressed in the literature. The first technique proposed was based on the polarimetric ratio of the peak of the waveform, which is the cross-correlation of the GNSS direct and reflected signals with a clean replica of the satellite code, or a Doppler cut in the DDM [11] passing through the DDM peak. GNSS signals are transmitted at RHCP, but in the reflection process they become mostly LHCP [11]. The power received at LHCP after reflection in a surface depends on the SM conditions [12]. If the LHCP component is expressed in the two orthogonal polarization components (V- and H-Pol), the SM can be estimated at each polarization. The ratio of the two should theoretically cancel surface roughness effects, but preserve the dielectric constant information [13]. However, due to surface roughness, there is a polarization mixing factor that must be considered. A similar approach is based on sensing the reflected power variations at LHCP from an airborne platform, as was the case of, for instance, the SMEX02 experiment [12], [14], where the received power increased with higher SM. Later, the ICF [15], which is a time series calculated as the ratio between the direct and the reflected waveform peaks, was used for the determination of the surface reflection coefficient [16]. From the estimated average reflection coefficient, the SM can be retrieved [16], [17]. The ICF has also been used with two nadir-looking antennas, one LHCP and another one RHCP, and a zenith-looking RHCP antenna for the direct signal. The polarimetric ratio of both estimated reflection coefficients is highly related to the biomass parameters [17].

Another approach known as the IPT has been followed by different researchers. The feasibility of sensing the complex dielectric constant using the multipath information from GPS SNR was proved in 1998 [18]. Since then, two different techniques using the IPT have been followed. The first one is based on using the multipath information from geodetic zenith-looking GPS antennas. The reflected signal is collected through the sidelobes of the antenna pattern, as it is out of the antenna beamwidth. Following the model presented in [19] and looking to the relative phase variations in the retrieved interference pattern, relative SM variations can be tracked [19]–[21]. The second technique, following [18], is based on measuring the IPT using a linear polarization antenna, particularly V-Pol [22]. With a V-Pol antenna looking at the horizon, which is forcing a 1-ray multipath, the minimum amplitude point or "notch," corresponds to the Brewster angle position. This can then be linked to the complex dielectric constant determination and thus to the SM content [23].

This work presents the generalization of the IPT using linear dual-polarization measurements instead of only V-Pol. In Section II, the IPT equations are reformulated to account for both V- and H-Pol. In Section III, an upgrade of the SMIGOL [22] instrument from V-Pol to Dual-Pol is presented. In Section IV, a SM retrieval algorithm from dual-polarization acquisitions is presented, discussed, and analyzed. In Section V, the first results from a ground-based experiment conducted in the Yanco area (Australia) are presented. Finally, Section VI presents the conclusion of this work.

II. Formulation of the IPT Equations for Dual-Pol Applications

GNSS signals are circularly polarized (RHCP), but after their reflection on a surface, they become mostly LHCP. A single RHCP antenna is not optimal for acquiring direct and reflected signals as those are orthogonal polarizations. Furthermore, the H-Pol component on the reflected signal masks the information of the Brewster angle position [24]. Consequently, the interference patterns used in this work are acquired using linear polarization. Linerly polarized antennas allow the acquisition of both direct and reflected signals with a single antenna. A linear dual-polarization antenna with a high cross-polar ratio allows the acquisition of the V- and H-Pol interference patterns with a single antenna.

The IPT is based on the coherent addition of direct and reflected GNSS signals. This results in an interference pattern (fading), with high- and low-frequency components. The high-frequency component is due to the phase difference or different path travelled by direct and reflected signals. The low-frequency component is due to the modulation by the antenna pattern and the reflection coefficient amplitude. Previously, the use of V-Pol was preferred due to the presence of the Brewster angle [22]. Using [22] and [24] as a start point, the potential of using H- and V-Pol at the same time to improve the accuracy of the SM retrieval is analyzed in this work.

In order to estimate the interference patterns at both polarizations, a model to compute the reflection coefficients must be used. Different reflection models have been proposed to estimate the reflection coefficients [25], [26]. In [22], a three-layer model was used: the first layer is the air ($\varepsilon_r \sim 1$); the second layer is a thin layer emulating the roughness, with a dielectric constant in between the one from the air layer and the one from the soil layer; the third layer is the soil layer. In this work, a two layer model has been used (Fig. 2), considering the surface roughness as an attenuation in the reflected wave [26]. No signicant differences have been found between the two- and three-layer models for relatively smooth terrains, which is the case of the experimental site.

A. The Fresnel Reflection Coefficients

The Fresnel reflection coefficients for H- and V-Pol are presented in (1)–(2). To consider the roughness effect, the reflectivity value (Γ_q) is multiplied by an exponential function [26], [27], (3)

$$R_{h_{1,2}} = \frac{\sqrt{1-sin^2(\theta_{inc})} - \sqrt{\varepsilon_{r_2} - sin^2(\theta_{inc})}}{\sqrt{1-sin^2(\theta_{inc})} + \sqrt{\varepsilon_{r_2} - sin^2(\theta_{inc})}} \quad (1)$$

$$R_{v_{1,2}} = \frac{\varepsilon_{r_2}\cdot\sqrt{1-sin^2(\theta_{inc})} - \sqrt{\varepsilon_{r_2} - sin^2(\theta_{inc})}}{\varepsilon_{r_2}\cdot\sqrt{1-sin^2(\theta_{inc})} + \sqrt{\varepsilon_{r_2} - sin^2(\theta_{inc})}} \quad (2)$$

$$\Gamma_q = |R_{q_{1,2}}|^2 \cdot e^{-4\cdot k^2\cdot {\sigma_h}^2\cdot \cos^2(\theta_{inc})} \quad (3)$$

where $R_{h_{1,2}}$ and $R_{v_{1,2}}$ are the Fresnel reflection coefficients for H- and V-Pol, respectively; 1 and 2 are the air and soil layers, respectively; ε_{r_2} is the dielectric constant of the soil layer; θ_{inc} is the incidence angle; q is the polarization (H-Pol or V-Pol); $k = \frac{2\pi}{\lambda}$, where λ is the wavelength (~ 19 cm); and, σ_h is the surface *rms* height.

Fig. 1 shows the reflectivity (Γ_q) for a) H- and b) V-Pol as a function of the incidence angle ($\theta_{inc} = 90^\circ - \theta_{elev}$), which is the complementary angle of the elevation (θ_{elev}). Note that the H-Pol reflectivity (Γ_H) is always monotonically increasing. On the contrary, the V-Pol reflectivity (Γ_V) value is decreasing until it reaches a minimum amplitude point, where it starts increasing. This minimum amplitude point is called "notch," and corresponds to the Brewster angle position. Note that, as stated in previous works [22], [24], its position mainly depends on the SM content. This means that V-Pol has a high sensitivity to the SM content, and it is the reason why V-Pol was chosen in previous works. For SM contents higher than 5%, the reflectivity value at the Brewster angle position is not equal to 0. This occurs because the real part of the reflection coefficients is almost zero, whereas the imaginary part is not. So, the amplitude does not vanish completely. Moreover, in the scattering area, the SM content is not homogeneous. In real cases, the reflectivity reaches a minimum value, which never becomes 0. Note that at V-Pol, two different SM contents may have the same Γ_V value. This leads to an ambiguity in the SM retrieval algorithm when a map is generated. This ambiguity is not seen at H-Pol and for $\theta_{elev} > 5^\circ$. Furthermore, Γ_H is always higher than Γ_V, being advantages of the dual-polarization technique.

The elevation angle region that can be analyzed is $5^\circ < \theta_{elev} < 45^\circ$ due to the antenna pattern half power beamwidth. Also, it is where the Brewster angle is located and Γ_H has higher values.

B. The Dual-Polarization Interference Patterns

The interference pattern equation [22] can be rewritten for H- and V-Pol using the reflection coefficients presented in Section II-A and an antenna ($F_n(\theta)$) with an azimutally symmetric pattern around the boresight (4)

$$P_R \propto |E_i + E_r|^2 = F_n(\theta_{elev}) \cdot |E_{0_i}|^2 \cdot |1 + |R_q(\theta_{elev}, \varepsilon_r)| \cdot e^{j(\Delta\phi + \phi_{R_q}(\theta_{elev}, \varepsilon_r))}|^2 \quad (4)$$

where

P_R	Instantaneous received/interference power;
E_i and E_r	Incident and reflected fields, respectively;
$F_n(\theta_{elev})$	Antenna radiation pattern;
E_{0_i}	Incident electric field amplitude;
$\lvert R_q(\theta_{elev}, \varepsilon_r)\rvert$	Absolute value of the Fresnel reflection coefficient at q polarization;
$\phi_{R_q}(\theta_{elev}, \varepsilon_r)$	Phase of the Fresnel reflection coefficient at q polarization;
$\Delta\phi = \frac{4\pi}{\lambda} h \sin(\theta_{elev})$	Phase difference due to the different electrical path between direct and scattered EM waves;
h	Height of the receiving antenna;
ε_r	Soil surface dielectric constant.

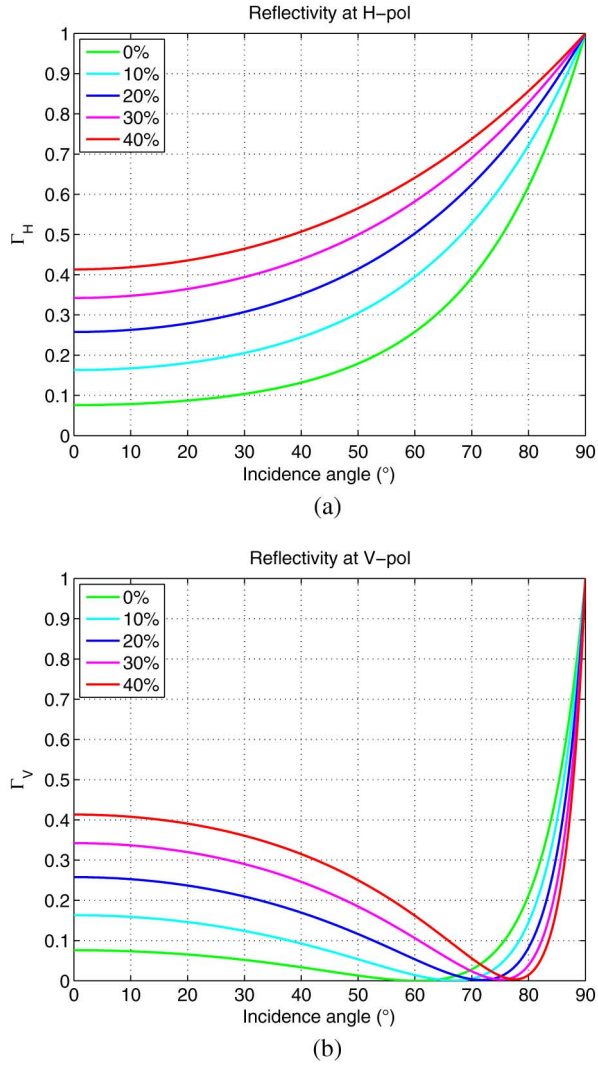

Fig. 1. Reflectivity as a function of SM. (a) H-Pol. (b) V-Pol.

Comparing (4) with prevoius formulation, the envelope of the interference pattern is now dominated by the absolute value of the reflection coefficient. The frequency modulation term is now $\Delta\phi + \phi_{R_q}(\theta, \varepsilon_r)$, which means that it depends on the different electrical path between direct and reflected signals and also on the reflection coefficient phase.

III. Dual-Polarization SMIGOL Instrument

The original SMIGOL reflectometer is a ground-based instrument that measures the IPT from GNSS direct and reflected signals. It has a vertically polarized antenna to measure the V-Pol interference pattern [24]. Fig. 2 shows the geometry of the SMIGOL instrument and the IPT.

For the demonstration of the dual-polarization concept, the instrument presented in [24] has been upgraded. The antenna has been modified for dual-polarization measurements and its pattern has been measured at the Universitat Politècnica de Catalunya-BarcelonaTech (UPC) anechoic chamber [28] confirming its

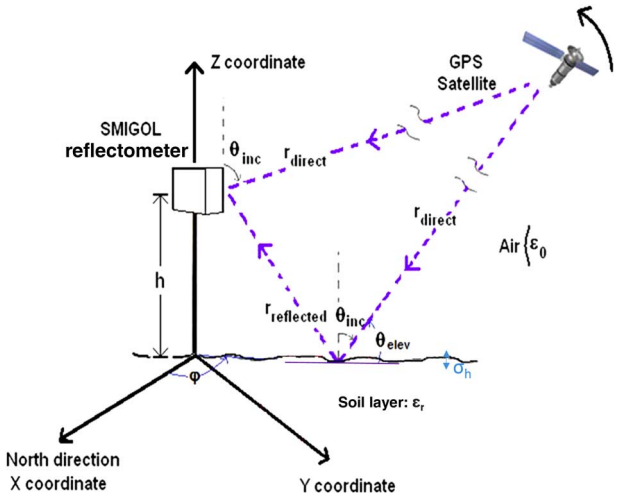

Fig. 2. Geometrical configuration of SMIGOL reflectometer and the GPS signals reflecting over a surface characterized by its dielectric constant (adapted from [24]).

symmetry at both polarizations, and ensuring a cross-polar ratio higher than 20 dB in any direction. The symmetry in the beamwidth is used to avoid antenna pattern compensations. The cross-polar relation is important to avoid receiving power from the nondesired polarization, which allows to safely apply dual-polarization algorithms.

After the antenna, there are identical RF amplifiers and receivers for each channel. The controlling system is in charge of internally referencing the data from each channel, and monitoring all the system parameters to keep the full system autonomy.

IV. Dual-Polarization SM Retrievals over Bare Soil

In previous works, in order to obatin a SM map, the amplitude measurements at V-Pol were adapted to the theoretical model as a function of the estimated SM value [24]. However, the aforementioned amplitude ambiguity of the reflection coefficient at V-Pol may lead to errors in the SM map. Furthermore, the larger the value of the reflection coefficient, the larger the amplitude oscillations of the IPT and consequently, the higher the amplitude sensitivity to SM variations. This is more noticeable at H-Pol than at V-Pol.

A. The Retrieval Algorithm

The new proposed algorithm uses the position of θ_B on the V-Pol interference pattern as a first estimation of the SM. Then, for the retrieval of the SM map, the amplitude of the interference pattern at H-Pol is used. Looking at (4), there are points of minima and maxima amplitude of the interference pattern. The minima points occur when the phase term is an odd multiple of π or $((2n+1)\pi = \Delta\phi + \phi_{R_q}(\theta, \varepsilon_r))$. The maxima amplitude points occur when the phase term is an even multiple of π or $(2n\pi = \Delta\phi + \phi_{R_q}(\theta, \varepsilon_r))$. So the maxima ($P_{q_{\max}}$) and minima ($P_{q_{\min}}$) power values are obtained according to (5) and (6), respectively

$$P_{q_{max}}(\theta_{elev}, \varepsilon_r) = F_n(\theta_{elev}) \cdot |E_{0_i}|^2 \cdot |1 + |R_q(\theta_{elev}, \varepsilon_r)||^2 \quad (5)$$

$$P_{q_{min}}(\theta_{elev}, \varepsilon_r) = F_n(\theta_{elev}) \cdot |E_{0_i}|^2 \cdot |1 - |R_q(\theta_{elev}, \varepsilon_r)||^2. \quad (6)$$

If the instrument height is higher than 3 m, the angular separation between consecutive maxima and minima is smaller than 1°. Considering that 1° angular variation in the absolute value of the reflection coefficient is negligible, the overall reflection coefficient at q polarization for a whole interference pattern can be estimated using (7)

$$|\hat{R}_q(\theta_{elev}, \varepsilon_r)| \approx \frac{\sqrt{\frac{P_{q_{max}}(\theta_{elev}, \varepsilon_r)}{P_{q_{min}}(\theta_{elev}, \varepsilon_r)}} - 1}{\sqrt{\frac{P_{q_{max}}(\theta_{elev}, \varepsilon_r)}{P_{q_{min}}(\theta_{elev}, \varepsilon_r)}} + 1}. \quad (7)$$

Equation (7) is an estimator of the reflection coefficient modulus, and consequently, by definition it will range between 0 and 1. Furthermore, there is a high similarity between (7) and the VSWR definition [29]. The VSWR in a microwave transmission line is the ratio between the maximum and the minimum voltages (V_{max}/V_{min}). If the transmission line is perfectly matched (ended with a matched load), there is no reflected wave and the VSWR value is 1, since $V_{max} = V_{min}$, which occurs at the θ_B position. However, if is not loaded, there is a reflected wave and the VSWR value is larger than 1. The load reflection coefficient absolute value and the VSWR are thus instrinsecally related [29]. A similarity between the IPT and the VSWR concept can be directly established. In the IPT, the observable are the power fluctuations of the incoming wave (direct) due to a mismatch of the reflecting medium (reflected wave). This happens because the transmission line/medium, in this case the air, is not perfectly matched (i.e., the soil layer is not a matched load for the air). Using this similarity, the VSWR concept is applied to extract an estimation of the reflection coefficient. A difference between the VSWR and the IPT is that, while the VSWR is a constant value for the whole transmission line, in the IPT case, as the reflection point changes due to the GNSS satellite movement, the soil properties may change, and consequently the reflection coefficient itself. This is why the reflection coefficient estimator depends on the elevation angle (θ_{elev}), and the soil dielectric properties (ε_r).

Summarazing, $|\hat{R}_q(\theta_{elev}, \varepsilon_r)|$ is an amplitude estimator of the Fresnel Reflection coefficient at different elevation angles at q polarization. From this estimation, it is straightforward to simulate different reflection coefficients for different ε_r and θ_{elev}. Consequently, ε_r estimates are linked to SM content at the different θ_{elev} values. This leads to spatial variability and the SM map.

B. System Limitations and SM Uncertainty Margins

Due to natural effects, such as surface roughness, or induced effects, such as quantization, there is an uncertainty in the estimation of the SM value.

First, quantization errors and noise lead to an uncertainty in the reflection coefficient amplitude estimation. The instrument measures the total received power (P_R, signal + noise). As the noise level is nearly constant, measuring the fluctuations of the received interference power is equal to measuring the fluctuations of the signal power. P_R is quantized in the instrument's receivers at steps of 1 dB. In the quantization, there is an intrinsic uncertainty of ± 0.5 dB. This leads to an uncertainty in the

reflection coefficient estimated. If the reflection coefficient estimator is given by (7), and considering the definition shown in (8), the uncertainty in the reflection coefficient estimation is given by (9)

$$u(\theta,\varepsilon_r) = 10^{\frac{P_{qmax}(\theta,\varepsilon_r)[dBau]-P_{qmin}(\theta,\varepsilon_r)[dBau]}{10}} \tag{8}$$

$$\Delta|\hat{R}_q(\theta,\varepsilon_r)| = \frac{ln10}{10}\frac{\sqrt{u}}{\left(\sqrt{u}+1\right)^2} \tag{9}$$

where $dBau$ is the measured total received power in arbitrary logarithmic units.

The uncertainty in the reflection coefficient estimation at H-Pol is translated into an uncertainty in the ε_r estimation. At H-pol, the dielectric constant (ε_{r_h}) uncertainty is given by

$$\Delta|\hat{\varepsilon}_{r_h}(\theta,\varepsilon_r)| = 4\cdot\frac{1+|\hat{R}_q(\theta,\varepsilon_r)|}{\left(1-|\hat{R}_q(\theta,\varepsilon_r)|\right)^3}\cdot\Delta|\hat{R}_q(\theta,\varepsilon_r)|. \tag{10}$$

Then, using Wang's model [23] to relate the SM content and the dielectric constant

$$\begin{aligned}\varepsilon_r = {} & 3.1 + 17.36\cdot SM + 63.12\cdot SM^2 \\ & + j\cdot(0.031 + 4.65\cdot SM + 20.42\cdot SM^2)\end{aligned} \tag{11}$$

the uncertainty in the SM retrieval is given by

$$\begin{aligned}\Delta SM = {} & \frac{1}{\sqrt{(17.36)^2 - 4\cdot 63.12\cdot(1-|\hat{\varepsilon}_{rh}(\theta,SM)|)}} \\ & \cdot\Delta|\hat{\varepsilon}_{rh}(\theta,SM)|.\end{aligned} \tag{12}$$

Table I shows a summary of the uncertainty budget propagation at H-Pol due to quantization. It covers the three steps; from the uncertainty in the estimation of the reflection coefficient up to the SM uncertainty. Note that the higher the SM content, the higher the reflection coefficient, the higher amplitude of the interference pattern, and the higher the dynamic range. Consequently, the lower is the quantization uncertainty effect on the reflection coefficient estimation. Different from the reflection coefficient estimation uncertainty, the uncertainty on ε_r increases with increasing SM values. Despite the uncertainty on the reflection coefficient decreases with increasing SM, the fact that the higher the SM, the higher the ε_r value compensates the decreasing factor and makes it increase. The same behaviour observed in the ε_r occurs in the uncertainty of the SM. The higher the uncertainty in the ε_r, the higher the uncertainty in the SM estimation.

For V-Pol, the uncertainty on the reflection coefficient due to the quantization is also given by (9). As the interference pattern dynamic range at V-Pol is smaller than at H-Pol, the uncertainty obtained will be slightly higher. However, a final expression for the dielectric constant inversion at V-Pol cannot be derived due to the amplitude ambiguity. This expresion changes as a function of the Brewster angle position, which is not known *a priori*.

TABLE I
UNCERTAINTY BUDGET SUMMARY TABLE DUE TO QUANTIZATION ERRORS (± 0.5 dB) AT H-POL

Soil moisture (%)	$\Delta\lvert\hat{R}_q(\theta,\varepsilon_r)\rvert$	$\Delta\lvert\hat{\varepsilon_{rh}}(\theta,\varepsilon_r)\rvert$	ΔSM (%)
0	0.0190	0.2755	1.5
10	0.0160	0.4878	1.7
20	0.0122	1.0772	2.4
30	0.0010	1.8189	3.0
40	0.0087	2.5582	3.5

Another aspect in the error estimation is the fitting between the dielectric constant model used and the real one. If the imaginary part is larger than the one predicted by the model, at the Brewster angle position, the reflection coefficient will have a minimum amplitude point, but not as close to 0. This is seen on the interference pattern as a "notch" with a larger amplitude. This also affects the H-Pol, just by a smaller amplitude uncertainty. In previous works, it has been seen that using the "notch" amplitude value as a SM content estimator with 1 dB quantization resolution, can provide uncertainties higher than 20% of SM value [22]. Therefore, the combination of both polarizations improves the accuracy of the SM retrievals as it will be shown with experimental data in Section V.

C. Theoretical Simulations

IPTs, with and without quantization errors, have been simulated to assess the retrieval algorithm performance. First, the IPT simulated for H- and V-Pol are shown in Fig. 3(a) and (b), respectively. As stated previously, the amplitude of the IPT envelope at H-Pol is larger than at V-Pol due to the difference in the reflection coefficient amplitude. Also, the presence of the Brewster angle is seen in Fig. 3(b) with its position varying as a function of the SM.

By applying the algorithm in (7), an estimation of the reflection coefficient at each polarization is obtained (Fig. 4). Notice that the retrieval has started at $\theta_{elev} = 5^\circ$, as for lower elevation angles, the dependance of the reflection coefficients on SM is not large enough to get a valuable retrieval. Moreover, an elevation angle mask in the PSMIGOL receivers avoids measuring power for too low elevation angles. In Fig. 4(b), the θ_B position is seen, as well as the amplitude ambiguity. At H-Pol, the whole range of elevation angles can be used for the retrieval [Fig. 4(a)].

From the estimated reflection coefficients, the SM at H-Pol has been inferred (Fig. 5), showing the evolution of the estimated SM as a function of the elevation angle. Table II shows the estimated SM value using the Brewster angle position information. As expected, V-Pol gives very precise information on the SM content. To characterize H-Pol information, a scatter plot representing the true SM values against the estimated SM values is presented in Fig. 6(a). A bias in the mean values of the SM estimation using H-Pol is observed. In order to compensate for this bias, the V-Pol Brewster angle information can be used as a reference value. Fig. 6(b) shows the corrected SM

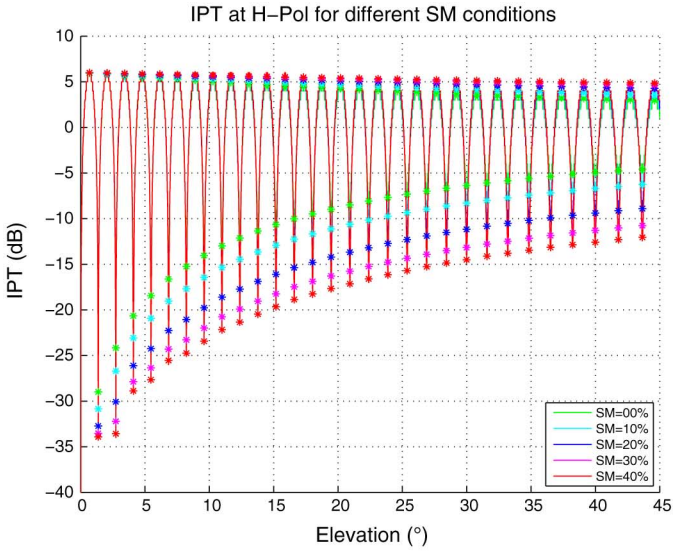

(a)

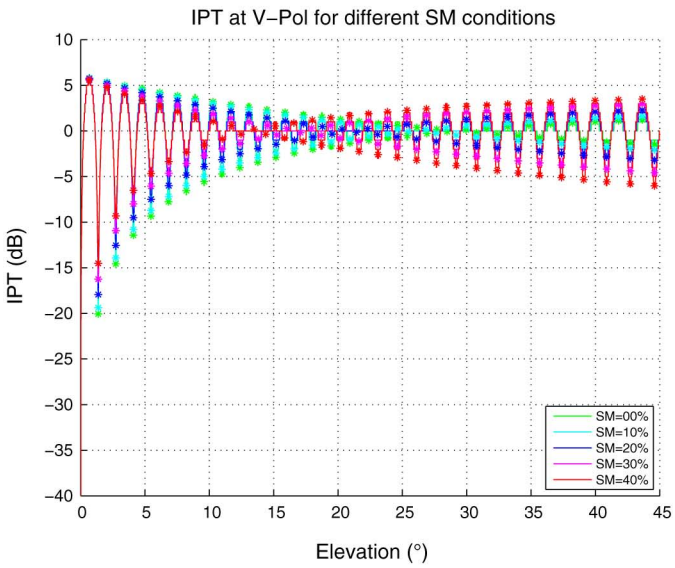

(b)

Fig. 3. IPT simulated at: (a) H- and (b) V-Pol for different SM values.

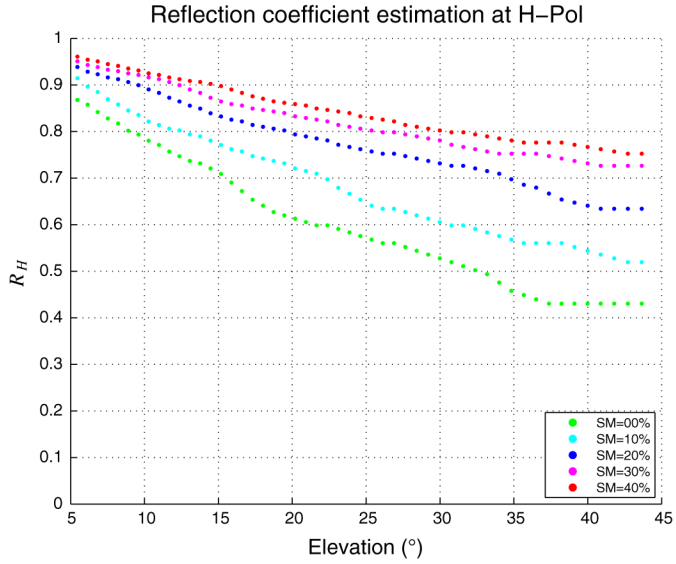

(a)

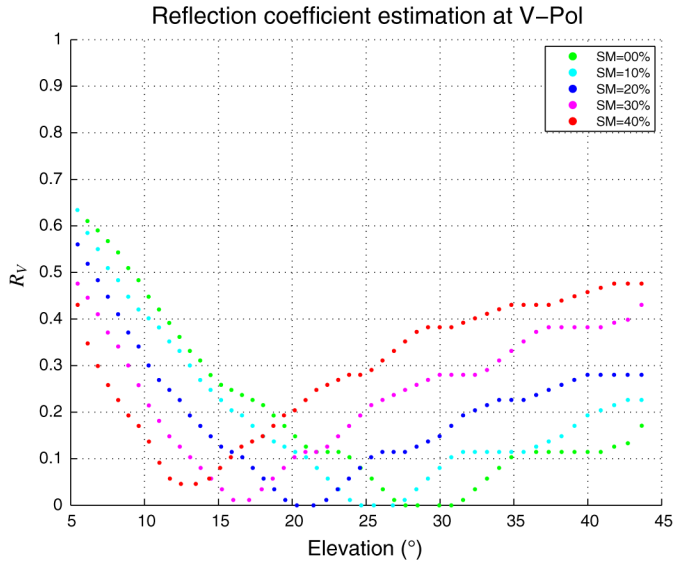

(b)

Fig. 4. Reflection coefficients retrieved from the IPT simulated at: (a) H- and (b) V-Pol for different SM values. Its accuracy is analyzed in Table III.

values retrieved. The presence of the bias has been reduced for $\mathrm{SM} > 5\%$. Conversely, for $\mathrm{SM} = 0\%$, the bias has been increased because the estimation of the Brewster angle position is not as accurate due to relatively high uncertainty of the dielectric constant. This can be seen in Fig. 4, where for $\mathrm{SM} = 0\%$ the minimum amplitude point ocupies a wide range of elevation angles. SM values are expected to vary from 5% (dry), 20% (moist), and 35% (wet).

In this section, the surface roughness parameter has been considered to be negligible. In real cases, as will be seen in Section V, it is not negligible. This effect is seen in the "notch" as a higher amplitude minimum not as close to 0.

In order to summarize the simulation analysis section, the theoretical mean and the standard deviation values of the simulated retrievals, in ideal case and with quantization, have been computed and presented in Table III.

V. Field Experiment: Real Data Analysis

In order to show the performance of the dual-polarization algorithm and the concepts proposed in this work, a field experiment was conducted at the Yanco, New South Wales, Australia field site of Monash University. The field experiment site is located within the OzNet SM monitoring network [30].

A. Field Experiment Setup

The PSMIGOL was installed on a wooden mast at a height of 3.6 m to avoid undesired reflections and multipath. In addition, the orientation of the antenna is in line (i.e., parallel) to the ground surface. As the surface conditions at this site are almost perfectly flat, both direct and reflected signals will have the same antenna gain. A fence was constructed surrounding the mast in

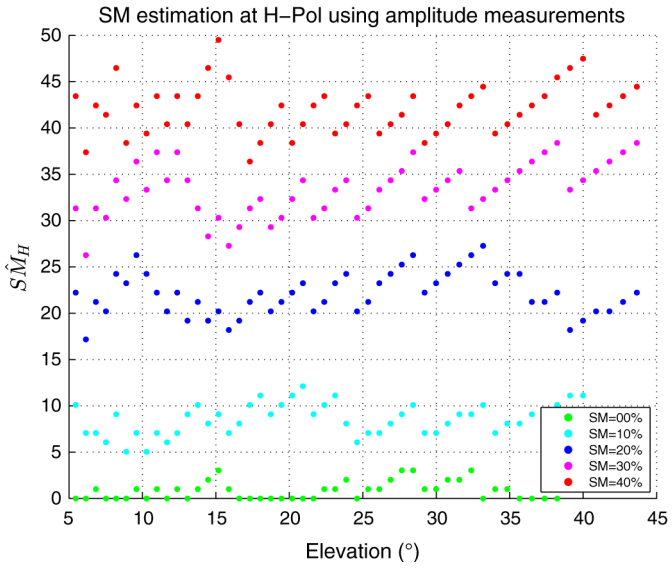

Fig. 5. SM estimation at H-Pol for different SM values using the amplitude of the IPT simulated taking into account the quantization effects.

TABLE II
COMPARISON BETWEEN TRUE SM AND SM RETRIEVAL USING THE BREWSTER ANGLE POSITION

True SM (%)	Estimated SM (%)
0	5.08
10	9.88
20	18.61
30	28.47
40	39.60

order to protect it from livestock present in the field. All fencing materials (posts, joints, pins, fence, and wire), as well as the mast itself and its restraints, are of nylon and wood. As those materials are nonreflective in the microwave spectrum, it was possible to avoid undesired reflections within the field of view of PSMIGOL. Fig. 7 shows the masthead with the PSMIGOL installation, along with the nylon wires (orange). Note that the PSMIGOL has the antenna covered by a radome, protecting it from harsh environmental conditions. It also has solar panels in order to give autonomy to the instrument. All the electronics were fitted inside an IP-66 gray box, where the antenna radome is glued.

B. Field Experiment Results

Fig. 8 shows the real data IPTs a) from GNSS PRN 1 on the July 16, 2013, and b) from the GNSS PRN 23 on the July 27, 2013. It is seen that the amplitude of the H-Pol IPT is larger than that from the V-Pol due to the larger reflection coefficient value. Both IPT, H- and V-Pol, are not aligned in none of the IPTs shown. This is due to the effect of having two phase terms in the IPT. One is related to the different path length of the direct and reflected signals, which is the same for both polarizations. The other term comes from the reflection coefficient phase at each polarization, which is different, and so it is the resultant phase of both IPT. The sensitivity to different surface points as the satellite

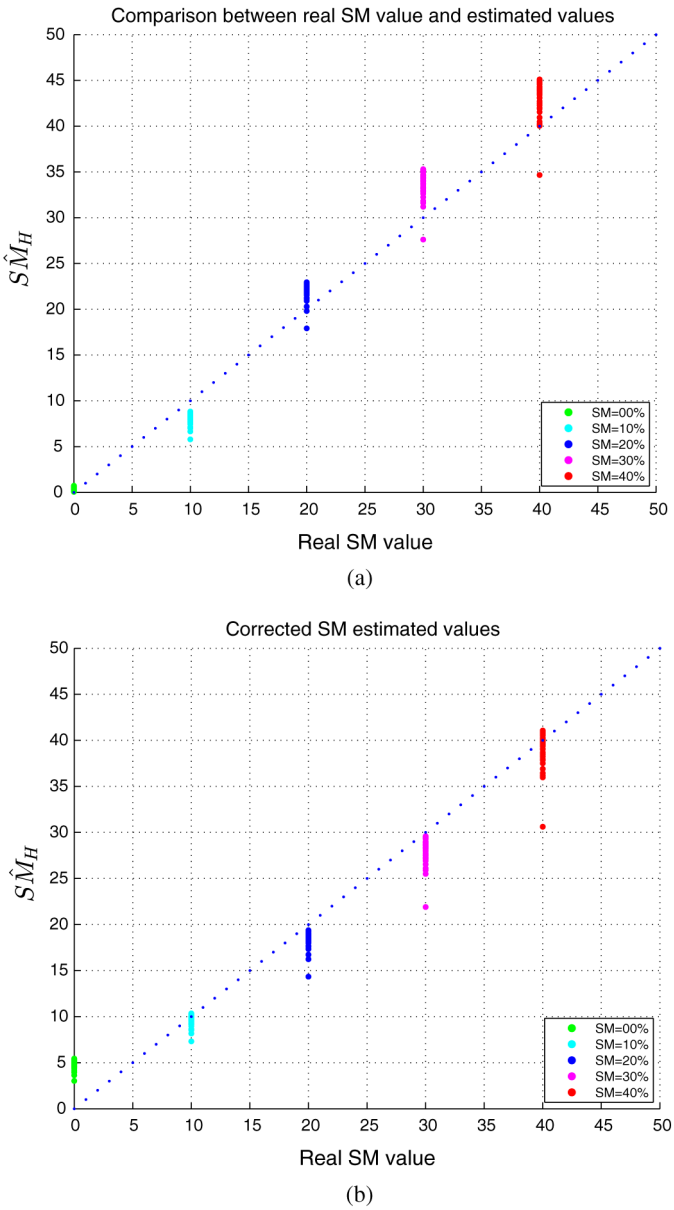

Fig. 6. Scatter plot of the true SM values (x-axis) against the estimated SM values (y-axis). The 1:1 line added to facilitate the comparison. (a) Estimated SM values. (b) Estimated and corrected SM values.

moves is also seen as the envelope of the IPT changes due to different elevation angles and SM conditions.

The absolute value of the reflection coefficient as a function of the elevation angle is extracted for both polarizations, by applying (7). From the reflection coefficient estimation, the SM values are inferred for each of the satellites as a function of the elevation angle. To do so, the θ_B is taken as a reference value, and then the H-Pol is used for the SM mapping. As seen in Fig. 9, where the θ_B SM estimation is marked in red and the blue marks are related to the H-Pol retrievals, the θ_B SM retrieval differs slightly from the mean value (22.1% and 14.1%, respectively) of the H-Pol retrievals.

Several IPTs retrieved between July 16th and July 31st have been analyzed. The data between the SM value retrieved using the Brewster angle information and the mean value of the

TABLE III
STATISTICS OF THE SIMULATED RETRIEVALS AT V- AND H-POL

SM (%)	H-Pol				H-Pol and V-Pol combined			
–	Ideal		Quantized		Ideal		Quantized	
–	Mean (%)	STD (%)	Mean (%)	STD (%)	Mean (%)	STD (%)	Mean (%)	STD (%)
0	0.89	0.32	1.01	1.02	5.08	0.32	5.08	1.02
10	8.79	0.51	8.77	1.58	9.89	0.51	9.89	1.58
20	21.9	0.57	22.09	2.22	18.62	0.57	18.62	2.22
30	33.58	0.87	33.49	2.77	28.46	0.87	28.46	2.77
40	42.67	1.09	42.08	2.69	39.6	1.09	39.6	2.69

Fig. 7. PSMIGOL on the mast at the Yanco Field Experiment site.

different point SM values using H-Pol for each satellite in view has been compared. Fig. 10 shows this comparison and a good linear fit ($R^2 = 0.895$ and $\mathrm{RMSE} = 2.2\%$) between both methods for estimating SM.

The last part of the data processing is to combine the data from different satellites to show the spatial and temporal diversities of the proposed technique. Fig. 11 shows the SM maps retrieved for a) July 16 and b) July 24, 2013. It shows the different reflection points due to satellite movement. Consequently, the SM values retrieved are different too. In addition, there are very close points corresponding to different satellites, from which SM estimated may differ by 10%. This aspect is related to the accuracy of the technique and the time difference between each sample was taken. This time difference can be up to 4 h with a rainfall occurring in between measurements.

C. Comparison Against Ground-Truth Data

The results obtained for different days between July 16 and July 31, 2013, have been compared with *in situ* SM instruments and rainfall events in that period. Fig. 12 shows a summary of

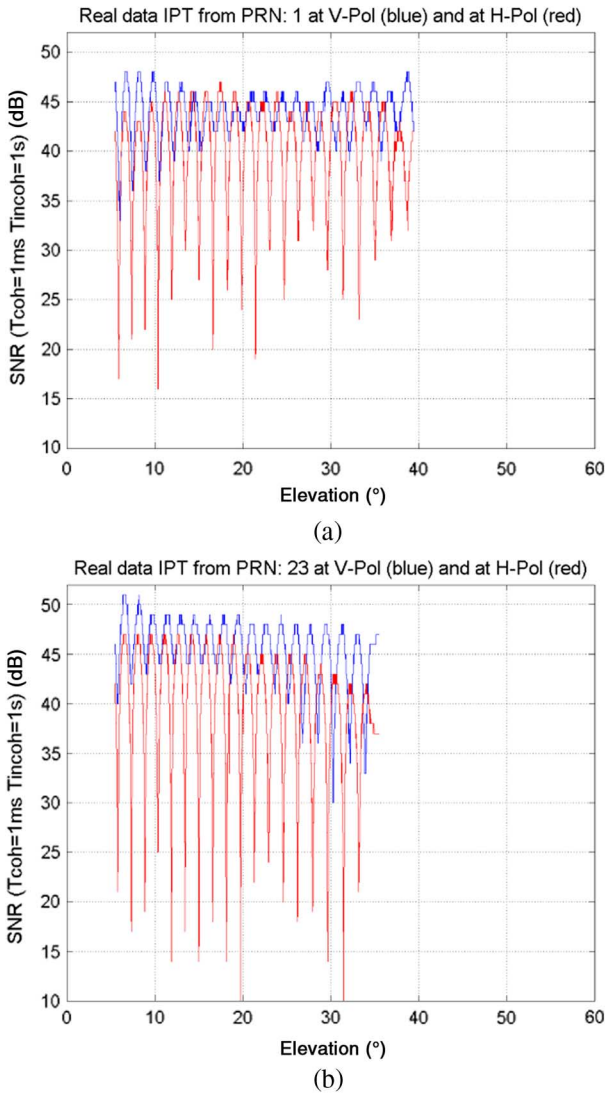

Fig. 8. Real data IPT retrieved, V-Pol (blue) and H-Pol (red). (a) 16th July 2013 (PRN: 1). (b) 27th July 2013 (PRN: 23).

the whole ground-truth information retrieved during the field experiment. The bars represent the rain events (in mm/day) from the closest information stations available: in blue the Yanco Agricultural Institute (YI) and in red the Narrandera Airport (NA). Rainfall information at those points is either collected with the traditional "Manual Rain Gauge," which is a manual measurement of the total amount of rain, or with the "Tipping Bucket Rain Gauge," an automatic measurement of the total amount of

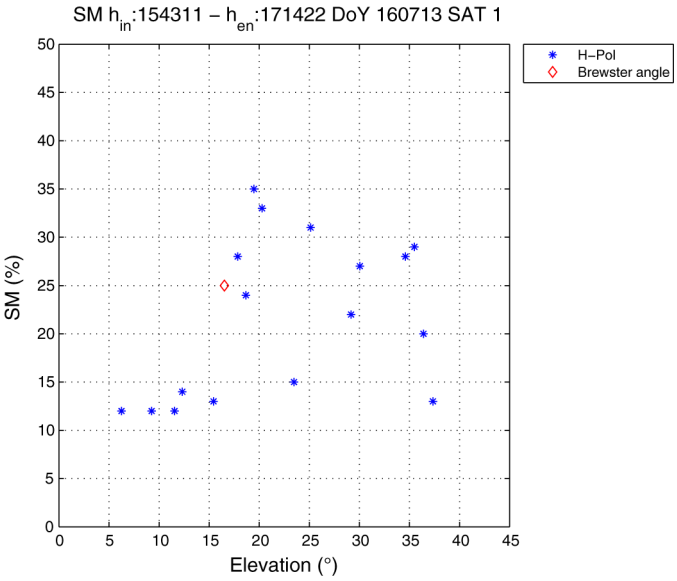

(a)

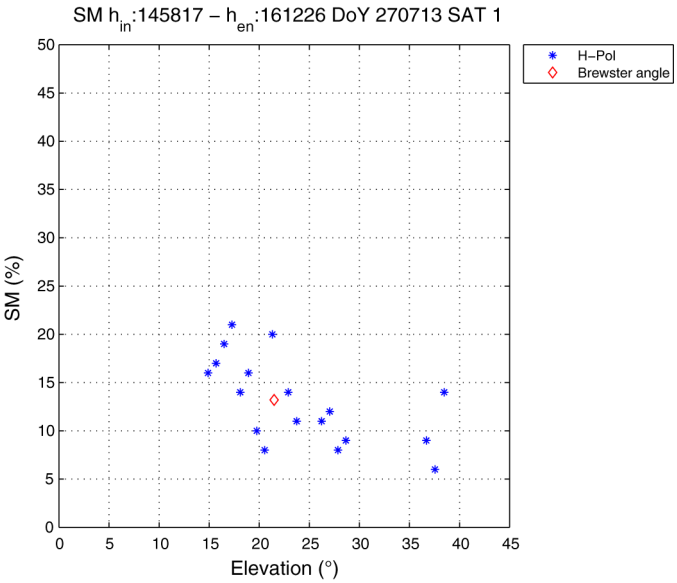

(b)

Fig. 9. SM retrieved from PRN1 on: (a) July 16 (PRN: 1) and (b) July 27, 2013 (PRN: 1). Red diamonds correspond to the Brewster angle SM estimation. Blue asterisks correspond to the H-Pol amplitude estimations of SM.

rain [31]. The SM measurements shown in Fig. 12 have been obtained with two different instruments: the Cosmic Ray Probe (CRP) and a SDI-12 SM probe. The CRP probe counts the number of neutrons emitted spontaneously by the soil to measure an area-average SM. The penetration depth of the CRP probe ranges between 10 and 25 cm, being lower for high SM values, and vice versa. The data shown from the CRP probe is a 12-h average of the time series data retrieved. The YB7 SM measurement station contains an SDI-12 SM probe [32], which provides point measurements of the top 5-cm volumetric SM content. The PSMIGOL instrument falls in the coverage area of the CRP sensor (200 m diameter), whereas the SDI-12 probe available is 700 m far away from the PSMIGOL.

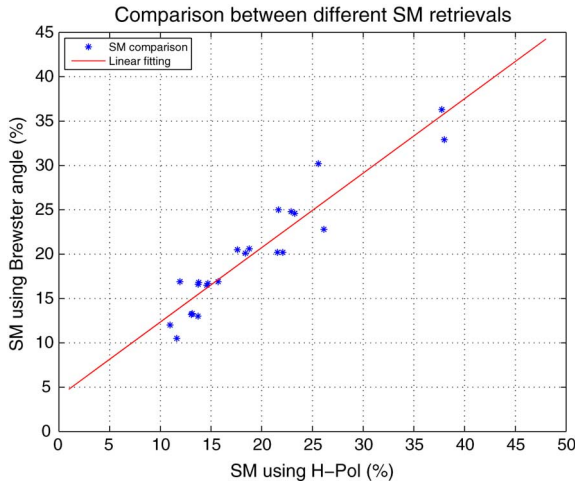

Fig. 10. Comparison between retrieved SM using the mean value of the H-Pol samples (x-axis) and the SM retrieved using the Brewster angle information (y-axis), $\mathrm{R}^2 = 0.895$ and $\mathrm{RMSE} = 2.2\%$.

(a)

(b)

Fig. 11. SM maps of: (a) July 16 and (b) July 24. The PSMIGOL instrument was situated in $\mathrm{Latitude} = 35.005613\mathrm{S}$, $\mathrm{Longitude} = 146.300523\mathrm{E}$.

The data obtained from the PSMIGOL instrument using either the mean value of the H-Pol information or the Brewster angle information are in between the data retrieved from both SM sensors. This agrees with the principles of the technique, being the penetration depth of the PSMIGOL instrument between 7 and 15 cm depending on the SM conditions. As the penetration depth of the PSMIGOL is higher than the SDI-12 and lower than the CRP sensor, it is expected to obtain SM values in between both sensors. It is also seen that after a rain

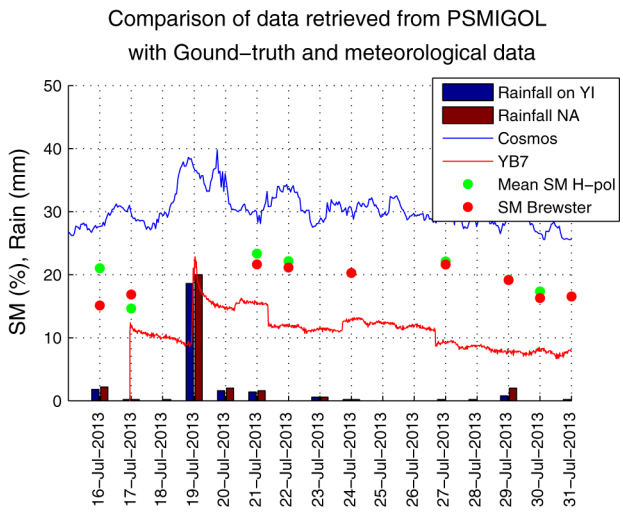

Fig. 12. Summary of the results obtained from the field campaign. Bars represent the rainfall events in millimeter/day. The blue bar shows the information of rain events from the YI. The red bar shows the information from the NA. The blue line shows the information from the Cosmos SM sensor (CRP, Cosmos). The red line shows the information of the YB7 SM probe. Green dots correspond to the mean SM value obtained from the H-Pol measurements. Red dots correspond to the mean SM value obtained from Brewster angle information.

event, SM increases and then it starts a decreasing trend as occurs in both CRP and SDI-12 sensors.

VI. Conclusion

This work has formulated the IPT equations for the dual-polarization case. The use of H-Pol helps to improve the accuracy of the estimated SM maps over bare soil or with very low vegetation (grass) scenarios. Although the Brewster angle position is a more accurate estimator of the average SM content at a determined position, H-Pol amplitude measurements are a better estimator away from the Brewster angle position, and eliminate the amplitude ambiguities of V-Pol.

An alternative method has been proposed for the estimation of the whole SM map, which is based on using the maxima and minima amplitude points of the IPT fast oscillations to retrieve a reflection coefficient image. The accuracy of this method is assessed including instrumental and modeling errors, showing that the range of elevation angles to be observed by the interference pattern is between 5° and 45°. The lower elevation angle is determined by the low dynamic range of the reflection coefficient amplitude, whereas the higher elevation angle is determined by the antenna pattern Beamwidth ($\Delta\theta_{-3\,\mathrm{dB}} \approx 45°$). Results from a field experiment conducted on Yanco, New South Wales, Australia, are presented showing a good agreement between the SM retrievals obtained using PSMIGOL and ground-truth.

Finally, to apply this technique, the cross-polar relationship of the antenna must be larger than 20 dB because, if the cross-polar relationship is not high enough, the "notch" can be masked due to the leakage between polarizations.

Acknowledgment

The authors thank F. Winston for his help in the installation and maintenance of P-SMIGOL at the experiment site.

References

[1] S. I. Seneviratne, T. Corti, E. L. Davin, M. Hirschi, E. B. Jaeger, I. Lehner, B. Orlowsky, and A. J. Teuling, "Investigating soil moisture–climate interactions in a changing climate: A review," *Earth-Sci. Rev.*, vol. 99, no. 3–4, pp. 125–161, 2010.

[2] L. Wang and J. Qu, "Satellite remote sensing applications for surface soil moisture monitoring: A review," *Frontiers Earth Sci. China*, vol. 3, no. 2, pp. 237–247, 2009.

[3] E. G. Njoku and D. Entekhabi, "Passive microwave remote sensing of soil moisture," *J. Hydrol.*, vol. 184, no. 1–2, pp. 101–129, 1996.

[4] A. Moccia and A. Renga, "Spatial resolution of bistatic synthetic aperture radar: Impact of acquisition geometry on imaging performance," *IEEE Trans. Geosci. Remote Sens.*, vol. 49, no. 10, pp. 3487–3503, Oct. 2011.

[5] E. Valencia, A. Camps, N. Rodriguez-Alvarez, H. Park, and I. Ramos-Perez, "Using GNSS-R imaging of the ocean surface for oil slick detection," *IEEE J. Sel. Topics Appl. Earth Observ. Remote Sens.*, vol. 6, no. 1, pp. 217–223, Feb. 2013.

[6] J.-C. Auber, A. Bibaut, and J.-M. Rigal, "Characterization of multipath on land and sea at GPS frequencies," in *Proc. 7th Int. Meet. Satell. Div. Inst. Navig. (ION GPS)*, Sep. 1994, pp. 1155–1171.

[7] M. Martín-Neira, "A passive reflectometry and interferometry system (PARIS): Application to ocean altimetry," *ESA J.*, vol. 17, pp. 331–355, 1993.

[8] S. Jin and A. Komjathy, "GNSS reflectometry and remote sensing: New objectives and results," *Adv. Space Res.*, vol. 46, no. 2, pp. 111–117, 2010.

[9] S. Jin, G. Feng, and S. Gleason, "Remote sensing using GNSS signals: Current status and future directions," *Adv. Space Res.*, vol. 47, no. 10, pp. 1645–1653, 2011.

[10] E. Cardellach *et al.*, "GNSS-R ground-based and airborne campaigns for ocean, land, ice, and snow techniques: Appications to the GOLD-RTR data sets," *Radio Sci.*, vol. 46, 2011.

[11] V. Zavorotny and A. Voronovich, "Scattering of gps signals from the ocean with wind remote sensing application," *IEEE Trans. Geosci. Remote Sens.*, vol. 38, no. 2, pp. 951–964, Mar. 2000.

[12] D. Masters, P. Axelrad, and S. Katzberg, "Initial results of land-reflected GPS bistatic radar measurements in SMEX02," *Remote Sens. Environ.*, vol. 92, no. 4, pp. 507–520, 2004.

[13] V. Zavorotny *et al.*, "Seasonal polarimetric measurements of soil moisture using tower-based GPS bistatic radar," in *Proc. IEEE Int. Geosci. Remote Sens. Symp. (IGARSS'03)*, 2003, vol. 2, pp. 781–783.

[14] S. J. Katzberg, O. Torres, M. S. Grant, and D. Masters, "Utilizing calibrated GPS reflected signals to estimate soil reflectivity and dielectric constant: Results from SMEX02," *Remote Sens. Environ.*, vol. 100, no. 1, pp. 17–28, 2006.

[15] G. Ruffini and F. Soulat, "On the GNSS-R interferometric complex field coherence time," ArXiv Physics e-prints, Jun. 2004.

[16] A. Egido *et al.* (2008). *Soil Moisture Monitorization Using GNSS Reflected Signals* [Online]. Available: http://arxiv.org/abs/0805.1881

[17] A. Egido *et al.*, "Global navigation satellite systems reflectometry as a remote sensing tool for agriculture," *Remote Sens.*, vol. 4, no. 8, pp. 2356–2372, 2012.

[18] A. Kavak, W. Vogel, and G. Xu, "Using GPS to measure ground complex permittivity," *Electron. Lett.*, vol. 34, pp. 254–255, 1998.

[19] V. Zavorotny *et al.*, "A physical model for GPS multipath caused by land reflections: Toward bare soil moisture retrievals," *IEEE J. Sel. Topics Appl. Earth Observ. Remote Sens.*, vol. 3, no. 1, pp. 100–110, Mar. 2010.

[20] K. Larson *et al.*, "GPS multipath and its relation to near-surface soil moisture content," *IEEE J. Sel. Topics Appl. Earth Observ. Remote Sens.*, vol. 3, no. 1, pp. 91–99, Mar. 2010.

[21] C. Chew, E. Small, K. Larson, and V. Zavorotny, "Effects of near-surface soil moisture on GPS SNR data: Development of a retrieval algorithm for soil moisture," *IEEE Trans. Geosci. Remote Sens.*, vol. 52, no. 1, pp. 537–543, Jan. 2014.

[22] N. Rodriguez-Alvarez *et al.*, "Soil moisture retrieval using GNSS-R techniques: Experimental results over a bare soil field," *IEEE Trans. Geosci. Remote Sens.*, vol. 47, no. 11, pp. 3616–3624, Nov. 2009.

[23] J. Wang and T. Schmugge, "An empirical model for the complex dielectric permittivity of soils as a function of water content," *IEEE Trans. Geosci. Remote Sens.*, vol. GE-18, no. 4, pp. 288–295, Oct. 1980.

[24] N. Rodriguez-Alvarez *et al.*, "Land geophysical parameters retrieval using the interference pattern GNSS-R technique," *IEEE Trans. Geosci. Remote Sens.*, vol. 49, no. 1, pp. 71–84, Jan. 2011.

[25] G. Lérondel and R. Romestain, "Fresnel coefficients of a rough interface," *Appl. Phys. Lett.*, vol. 74, no. 19, 1999.

[26] B. J. Choudhury, T. J. Schmugge, A. Chang, and R. W. Newton, "Effect of surface roughness on the microwave emission from soils," *J. Geophys. Res.: Oceans*, vol. 84, no. C9, pp. 5699–5706, 1979.

[27] P. Beckmann and A. Spizzichino, *The Scattering of Electromagnetic Waves from Rough Surfaces*. New York, NY, USA: Pergamon, 1993.
[28] AntennaLab [Online]. Available: http://www.tsc.upc.edu/antennalab/
[29] D. M. Pozar, *Microwave Engineering*, 4th ed. Hoboken, NJ, USA: Wiley, 2012.
[30] A. B. Smith *et al.*, "The Murrumbidgee soil moisture monitoring network data set," *Water Resour. Res.*, vol. 48, 2012.
[31] Bureaou of meteorology. *Bureaou of meteorology: Measuring rainfall in Australia*. Available: http://www.bom.gov.au/climate/cdo/about/definitionsrain.shtml#meanrainfall.
[32] Stevens Water Monitoring Systems, Inc. *SDI-12 SM probe*. Available: http://www.oznet.org.au/SDI-12.html.

Alberto Alonso Arroyo (S'11) was born in Barcelona, Spain. He received the M.S. degree in telecommunications engineering and the M.S. degree in research on information and ommunication technologies from the Universitat Politècnica de Catalunya–BarcelonaTech, Barcelona, Spain, in 2011 and 2012, respectively. Currently, he is pursuing the Ph.D. degree in GNSS-reflectometry with the Passive Remote Sensing Group, Department of Signal Theory and Communications, Universitat Politècnica de Catalunya–BarcelonaTech.

Adriano Camps (S'91–A'97–M'00–SM'03–F'11) was born in Barcelona, Spain, in 1969. He received the degree in telecommunications engineering and the Ph.D. degree in telecommunications engineering from the Universitat Politècnica de Catalunya (UPC), Barcelona, Spain, in 1992 and 1996, respectively.

In 1991 to 1992, he was at the ENS des Télécommunications de Bretagne, France, with an Erasmus Fellowship. Since 1993, he has been with the Electromagnetics and Photonics Engineering Group, Department of Signal Theory and Communications, UPC, where he was first Assistant Professor, Associate Professor in 1997, and Full Professor since 2007. He has published more than 125 peer-reviewed journal papers, and more than 250 international conference presentations.

Dr. Camps received a number of awards for his research and teaching activies, among which the Research Distinction of the Generalitat de Catalunya in 2002 for contributions to microwave passive remote sensing; the European Young Investigator Award in 2004 of the European Science Foundation; the ICREA Academia award in 2009; and the 1st Duran Farell Awards in 2000 and 7th Duran Farell Awards in 2010.

Albert Aguasca (S'90–M'94) was born in Barcelona, Spain, in 1964. He received the M.Sc. and Ph.D. degrees in telecommunication engineering from the Universitat Politècnica de Catalunya (UPC), Barcelona, Spain, in 1989 and 1993, respectively.

Since 1995, he has been an Associate Professor with the School of Telecommunications Engineering, UPC. He has published more than 40 papers on microwave synthetic aperture radar, radiometer systems, and microwave circuits. His research interests include design and development of synthetic aperture radar and microwave radiometer systems for unmanned aerial vehicle (UAV) platforms.

Giuseppe F. Forte (M'11) was born in Guatemala City, Guatemala, in 1979. He received the M.Sc. degree in electronics engineering form the Universidad Francisco Marroquín (UFM), Guatemala City, Guatemala, in 2002. In 2005, he received the advanced studies in electronic engineering diploma from the Universitat Rovira i Virgili (URV), Tarragona, Spain. Currently, he is pursuing the Ph.D. degree in telecommunications engineering at the Universitat Politècnica de Catalunya (UPC), Barcelona, Spain.

Since 2010, he has been involved in the Remote Sensing Laboratory (RSLAB), UPC, performing the design and implementation of algorithms, electronics, and field experiments related to remote sensing and radio frequency interference detection and mitigation.

Alessandra Monerris (S'04–M'09) received the B.E. degree in telecommunication from the Universitat Politècnica de València, València, Spain, and the Ph.D. degree in electrical engineering from the Universitat Politècnica de Catalunya, Barcelona, Spain.

In 2006, she was a Visiting Ph.D. student with the Universita Tor Vergata, Rome, Italy. From 2007 to 2011, she was Executive Director with the Soil Moisture and Ocean Salinity Expert Centre, Barcelona (SMOS-BEC), Spain. Currently, she is a Research Fellow with the Department of Civil Engineering, Monash University, Melbourne, Australia. She is also managing the OzNet soil moisture monitoring network in the Murrumbidgee River Catchment, Australia. Her research interests include estimation of soil moisture and vegetation parameters from L-band passive observations, cosmic-ray probes, and Global Navigation Satellite Systems Reflectometry (GNSS-R).

Cristoph Rüdiger (M'10) received the B.E. degree in civil engineering from the University of Applied Sciences, Wiesbaden, Germany, in 2002, and the Ph.D. degree in environmental engineering from the University of Melbourne, Melbourne, Australia, in 2007.

Currently, he is a Lecturer with Monash University, Melbourne, Australia. In 2007, he joined the Centre National de Recherches Météorologiques (CNRM), Météo France, Toulouse, France, to work on the preparation of surface soil moisture and LAI data assimilation into the French land surface model ISBA. Since his return to Australia in July 2008, he has coordinated and led a number of cal/val campaigns for the Australian land validation segment of SMOS mission in the Australian arid zone and the Murrumbidgee River catchment. In addition to this, he continues to work on land surface data assimilation and also participates in the Australian cal/val segments for NASA's SMAP and Aquarius. His research interests include remote sensing of vegetation dynamics and landscape water content.

Jeffrey P. Walker received the B.E. degree in civil and the B.Surv. degree (Hons. 1 and University Medal) from the University of Newcastle, Newcastle, Australia, in 1995, and the Ph.D. degree in water resources engineering from the University of Newcastle, in 1999.

He then joined NASA Goddard Space Flight Centre to implement his soil moisture work globally. In 2001, he moved to the Department of Civil and Environmental Engineering, the University of Melbourne, Melbourne, Australia, as a Lecturer, where he continued soil moisture work, including development of the only Australian airborne capability for simulating new satellite missions for soil moisture. In 2010, he was appointed as a Professor with the Department of Civil Engineering, Monash University, Melbourne, Australia, where he is continuing this research. He is contributing to soil moisture satellite missions at NASA, ESA, and JAXA, as a Science Team Member for the Soil Moisture Active Passive (SMAP) mission and cal/val Team Member for the Soil Moisture and Ocean Salinity (SMOS), and Global Change Observation Mission-Water (GCOM-W), respectively.

Hyuk Park (S'05–AM'09–M'12) was born in South Korea. He received the B.S. degree in mechanical engineering from the Korea Advanced Institute of Science and Technology (KAIST), Daejeon, South Korea, in 2001, and received the M.S. and Ph.D. degrees in information and mechatronics from the Gwangju Institute of Science and Technology (GIST), Gwangju, South Korea, in 2003 and 2009, respectively.

In 2009, he joined as a Postdoctoral Researcher in the Remote Sensing Group, the Polytechnic University of Catalonia (UPC), Barcelona, Spain. From 2012, he has been working as a Research Associate with Grant of Juan de la Cierva funded by Spanish Ministry of Economy and Competitiveness. Currently, he is working with the Passive Remote Sensing Group, the UPC for satellite remote sensing for microwave radiometry and GNSS-R. His research interests include area of remote sensing, especially passive microwave remote sensing, including system design, modeling and simulation, and image processing.

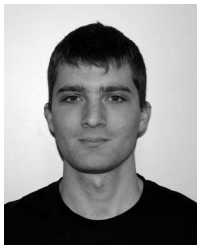

Daniel Pascual (S'11) was born in Barcelona, Spain, in 1985. He received the B.Sc. degree in telecommunications engineering specialized in communications and the M.Sc. degree in research on information and communication technologies from the Universitat Politècnica de Catalunya (UPC), Barcelona, Spain, in 2011 and 2014. In 2011, he joined the Passive Remote Sensing Group from UPC, where he is currently pursuing the Ph.D. degree in GNSS-Reflectometry focused in ocean altimetry.

Raul Onrubia (S'10) was born in Barcelona, Spain. He received the M.S. degree in telecommunications engineering and is currently pursuing the M.S.degree in research on information and communication technologies at Universitat Politécnica de Catalunya, Barcelona, Spain.

His research interest includes RF systems and hardware developing in the GNSS-Reflectometry in the Passive Remote Sensing Group at the Signal Theory and Communications Department.